International Workshop on Hadron Structure and Spectroscopy
IWHSS2022 – CERN, August 2022

F Hautmann

Nonperturbative Contributions to Semi-Inclusive Deep Inelastic Scattering and Drell-Yan Transverse Momentum Spectra: PDF Bias and Flavor Dependence in TMD Distributions

based on Phys. Lett. B 806 (2020) 135478 [arXiv:2002.12810],
arXiv:2201.07114

thanks to collaborators M. Bury, S. Leal Gomez,
I. Scimemi, A. Vladimirov, P. Zurita

TRANSVERSE MOMENTUM SPECTRA AT LOW qT

- It was realized long ago that transverse momentum qT spectra, in hard processes at scale Q in hadron collisions, are affected for qT << Q by large dynamical effects beyond collinear factorization:

  - perturbative logarithmically-enhanced corrections in

$$\alpha_s^n \ln^m Q/q_T$$

  - nonperturbative contributions besides PDFs due to

    i) intrinsic kT distribution of initial states and

    ii) nonperturbative components of Sudakov form factors.

[Parisi-Petronzio, NPB 154 (1979) 427
Curci-Greco-Srivastava, NPB 159 (1979) 451
Dokshitzer-Diakonov-Troian, Phys Rep 58 (1980) 269
Collins-Soper, NPB 193 (1981) 381]

LOW-qT FACTORIZATION AND EVOLUTION

[Collins-Soper-Sterman, NPB 250 (1985) 199;

Collins, Foundations of perturbative QCD, CUP 2011]

We start from the TMD factorization formula for the differential cross section for DY lepton pair production $h_1 + h_2 \to Z/\gamma^*(\to ll') + X$ at low $q_T \ll Q$ [13]

$$\frac{d\sigma}{dQ^2 dy dq_T^2} = \sigma_0 \sum_{f_1,f_2} H_{f_1 f_2}(Q,\mu) \int \frac{d^2\boldsymbol{b}}{4\pi} e^{i\boldsymbol{b}\cdot\boldsymbol{q}_T} F_{f_1\leftarrow h_1}(x_1,\boldsymbol{b};\mu,\zeta_1) F_{f_2\leftarrow h_2}(x_2,\boldsymbol{b};\mu,\zeta_2) + O(q_T/Q) + O(\Lambda_{\rm QCD}/Q), \quad (1)$$

where Q^2, $\boldsymbol{q}_T$ and y are the invariant mass, transverse momentum and rapidity of the lepton pair, and the TMD distributions $F_{f\leftarrow h}$ fulfill evolution equations in rapidity

$$\frac{\partial \ln F_{f\leftarrow h}}{\partial \ln \zeta} = -\mathcal{D}^f(\mu,\boldsymbol{b}) \quad (2)$$

and in mass

$$\frac{\partial \ln F_{f\leftarrow h}}{\partial \ln \mu} = \gamma_F(\alpha_s(\mu),\zeta/\mu^2) \ , \qquad \frac{\partial \mathcal{D}^f(\mu,\boldsymbol{b})}{\partial \ln \mu} = \frac{1}{2}\Gamma_{\rm cusp}(\alpha_s(\mu)) \ . \quad (3)$$

PHENOMENOLOGICAL STUDIES OF NONPERTURBATIVE TMD EFFECTS

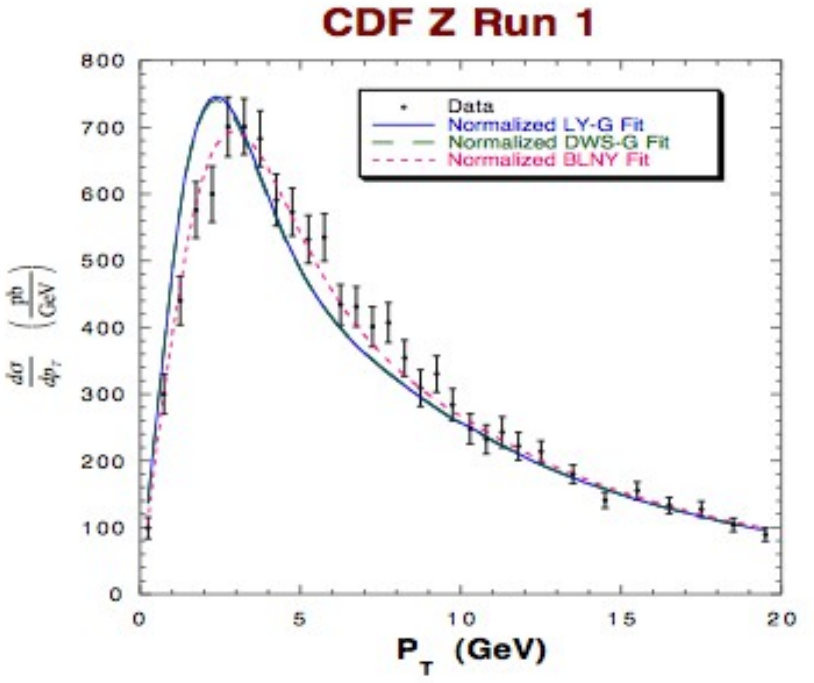

- Pioneering studies by “Resbos”:

[Ladinsky-Yuan, PRD 50 (1994) R4239
Landry et al, PRD 63 (2001) 013004
Landry et al, PRD 67 (2003) 073016
Konychev-Nadolsky, PLB633 (2006) 710]

- Recent “TMD fits”:

Scimemi-Vladimirov, JHEP 06 (2020) 137; Bacchetta et al., JHEP 07 (2020) 117, arXiv:2206.07598

- “Parton branching TMD” determination:

Bermudez Martinez et al., Phys. Rev. D 99 (2019) 074008

EXAMPLE: RECENT DETERMINATIONS OF RAPIDITY EVOLUTION KERNEL *D (b, mu)*

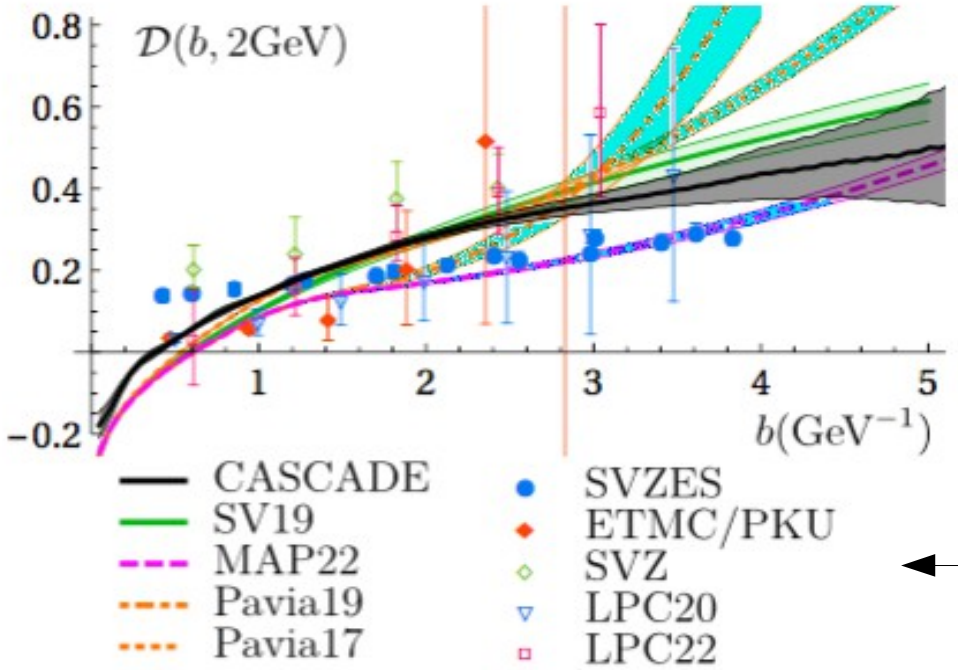

A Bermudez Martinez and A Vladimirov, arXiv:2206.01105

Determinations of kernel *D* from different approaches:
- fits to experimental data;
- lattice calculations;
- TMD Monte Carlo calculations.

NB: determinations of *D* from data fits in this figure assume either quadratic (a la Resbos) or linear behavior in *b* at large *b.* The alternative possibility of constant behavior at large *b* is studied in arXiv:2002.12810, arXiv:2109.12051 (similar in spirit to 's-channel picture' [Soper & H, PRD 75 (2007) 074020]).

- This talk will concentrate on studies (based on arXiv:2201.07114) to assess TMD uncertainties in current extractions from fits to experimental data.

A purely factorization-based approach to TMD extraction

Factorization formula of schematic form (up to power corrections):

$$\frac{d\sigma}{dq_T^2} = \sum_{i,j} \int d^2b\, e^{ib\cdot q_T}\, \sigma_{ij}^{(0)}\, f_{1,i\leftarrow h1}(x_1, b; \mu, \zeta_1)\, f_{1,j\leftarrow h2}(x_2, b; \mu, \zeta_2)$$

+ appropriate evolution equations for the TMD distributions *f*

- Measure observable on left hand side; extract *f* on right hand side
- *f* nonperturbative quantity, determined with experimental uncertainties (due to data) and theoretical uncertainties (due to factorization and evolution)

- This would be in the spirit of
  Jung, Mulders, Kraemer, Nocera, Rogers, Signori & H,
  "TMDlib", Eur. J. Phys. C 74 (2014) 3220 [arXiv:1408.3015]

Extraction of TMD distributions using OPE relations

- OPE: *f* is expanded along collinear PDFs, with *b^2* power corrections

$$f_{1,f\leftarrow h}(x,b;\mu,\zeta) = \sum_{f'} \int_x^1 \frac{dy}{y} C_{f\leftarrow f'}(y,b;\mu,\zeta)\, q_{f'}\left(\frac{x}{y},\mu\right) + O(b^2)$$

- Ansatz is made for the large-*b*, nonperturbative *f_NP*

$$f_{1,f\leftarrow h}(x,b;\mu,\zeta) = \sum_{f'} \int_x^1 \frac{dy}{y} C_{f\leftarrow f'}(y,b;\mu,\zeta)\, q_{f'}\left(\frac{x}{y},\mu\right) f^f_{\rm NP}(x,b)$$

and *f_NP* is fitted.

- "PDF bias" (an *f_NP* for every PDF set or PDF replica)

- fits so far include flavor dependence in PDF but not in *f_NP*

- We address these two issues next.

STRATEGY (I)

[Bury et al., arXiv:2201.07114]

- Take PDF sets HERA2.0, NNPDF3.1, CT18 and MSHT20, representative of different methodological approaches at NNLO
- Perform fits to unpolarized DY production at small qT, from fixed-target to LHC energies
- Use a Bayesian procedure to propagate PDF uncertainties, for each PDF set, to TMD extractions
- Obtain results for the fitted NP TMD distributions which display, for the first time, both experimental and PDF uncertainties.

STRATEGY (II)

[Bury et al., arXiv:2201.07114]

- Go beyond the assumption of flavor-independent *f_NP* used so far in the literature, and include flavor dependence in NP TMD distributions.

  To this end we will use the parameterization

$$f_{\rm NP}^f = \exp\left(-\frac{(1-x)\lambda_1^f + x\lambda_2^f}{\sqrt{1+\lambda_0 x^2 b^2}} b^2\right)$$

- Assess the impact of flavor dependence on fits: study the distribution of chi-squared values over PDF replicas, for each PDF set, in the flavor-dependent case compared to the flavor-independent case; examine the consistency of results across different collinear PDF sets.

INCLUSION OF PDF UNCERTAINTY AND FLAVOR DEPENDENCE IN TMD EXTRACTION

[Bury, Leal Gomez, Scimemi, Vladimirov, Zurita & H, arXiv:2201.07114]

- TMD-factorized DY formula implemented in `artemide` at NNLL';
  collinear sets from `LHAPDF`;
  minimization by `iMinuit`.

- Represent PDF as MC ensemble
- Uncertainties by fitting each member of input ensemble
- Two uncertainty sources, EXP and PDF

$$\delta \equiv \frac{\langle q_T \rangle}{\langle Q \rangle} < 0.1, \quad \text{or} \quad \delta < 0.25 \quad \text{if} \quad \delta^2 < \sigma$$

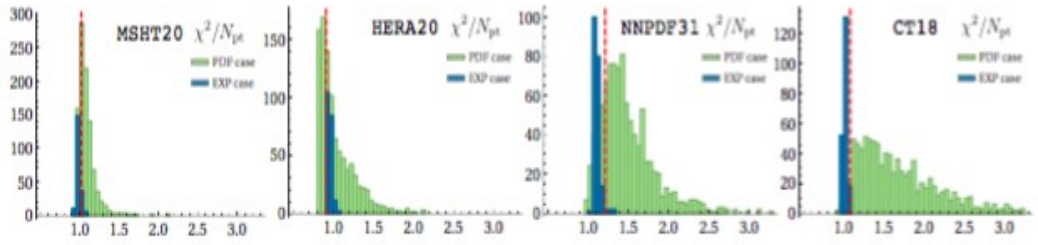

Figure 5: Distribution of χ^2-values for the **PDF** and **EXP** cases. The red lines show the position of the final χ^2-value.

		MSHT20	HERA20	NNPDF31	CT18
Data set	N_{pt}	χ^2/N_{pt}	χ^2/N_{pt}	χ^2/N_{pt}	χ^2/N_{pt}
CDF run1	33	0.78	0.61	0.72	0.75
CDF run2	39	1.70	1.42	1.68	1.79
D0 run1	16	0.71	0.81	0.79	0.79
D0 run2	8	1.95	1.39	1.92	2.00
D0 run2 (μ)	3	0.50	0.59	0.55	0.52
ATLAS 7TeV 0.0<|y|<1.0	5	4.06	1.94	2.12	4.21
ATLAS 7TeV 1.0<|y|<2.0	5	7.78	4.83	4.52	6.12
ATLAS 7TeV 2.0<|y|<2.4	5	2.57	2.18	3.65	2.39
ATLAS 8TeV 0.0<|y|<0.4	5	2.98	3.66	2.12	3.23
ATLAS 8TeV 0.4<|y|<0.8	5	2.00	1.53	4.52	3.21
ATLAS 8TeV 0.8<|y|<1.2	5	1.00	0.50	2.75	1.89
ATLAS 8TeV 1.2<|y|<1.6	5	2.25	1.61	2.49	2.72
ATLAS 8TeV 1.6<|y|<2.0	5	1.92	1.68	2.86	1.96
ATLAS 8TeV 2.0<|y|<2.4	5	1.35	1.14	1.47	1.06
ATLAS 8TeV 46<Q<66GeV	3	0.59	1.86	0.23	0.05
ATLAS 8TeV 116<Q<150GeV	7	0.61	1.03	0.85	0.70
CMS 7TeV	8	1.22	1.19	1.30	1.25
CMS 8TeV	8	0.78	0.77	0.75	0.78
CMS 13TeV 0.0<|y|<0.4	8	3.52	1.93	2.13	3.73
CMS 13TeV 0.4<|y|<0.8	8	1.06	0.53	0.71	1.65
CMS 13TeV 0.8<|y|<1.2	10	0.48	0.14	0.33	0.88
CMS 13TeV 1.2<|y|<1.6	11	0.62	0.33	0.47	0.86
CMS 13TeV 1.6<|y|<2.4	13	0.46	0.32	0.39	0.57
LHCb 7TeV	8	1.79	1.00	1.62	1.16
LHCb 8TeV	7	1.38	1.29	1.63	0.83
LHCb 13TeV	9	1.28	0.84	1.07	0.93
PHE200	3	0.29	0.42	0.38	0.29
E228-200	43	0.43	0.36	0.57	0.43
E228-300 Q < 9GeV	43	0.77	0.56	0.89	0.55
E228-300 Q > 11GeV	10	0.29	0.37	0.45	0.44
E228-400 Q < 9GeV	34	2.19	1.15	1.49	1.34
E228-400 Q > 11GeV	42	0.25	0.61	0.44	0.40
E772	35	1.14	1.37	1.79	1.11
E605 Q < 9GeV	21	0.52	0.47	0.47	0.61
E605 Q > 11GeV	32	0.47	0.73	1.34	0.52
Total	**507**	**1.12**	**0.91**	**1.21**	**1.08**

Table 3: Distribution of the values of χ^2 over the TMD data set in fits with different PDF input.

Flavour dependence of the TMDs

flavor-independent case

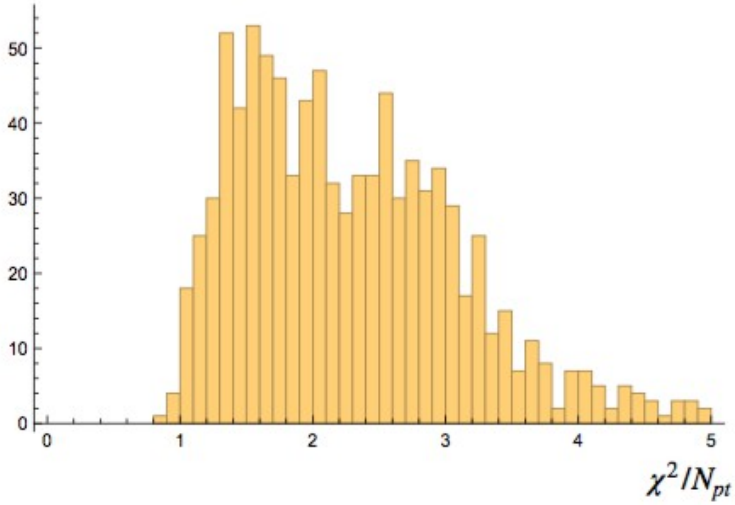

flavor-dependent

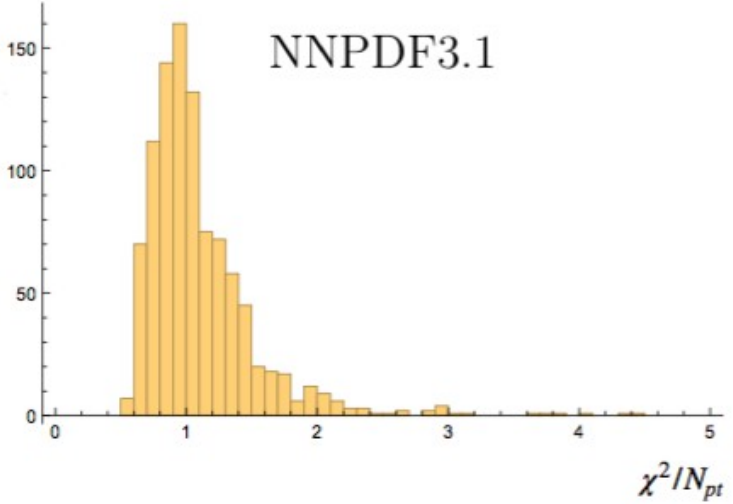

$$f_{NP}(x,b) = \exp\left(-\frac{\lambda_1(1-x)+\lambda_2 x + x(1-x)\lambda_5}{\sqrt{1+\lambda_3 x^{\lambda_4}\mathbf{b^2}}}\mathbf{b^2}\right)$$

$$f^f_{NP}(x,b) = \exp\left(-\frac{\lambda^f_1(1-x)+\lambda^f_2 x}{\sqrt{1+\lambda_0 x^2\mathbf{b^2}}}\mathbf{b^2}\right)$$

$f = u, \bar{u}, d, \bar{d}, sea$

- The figure above is obtained with the NNPDF3.1 set. We have verified that similar features hold for all PDF sets.

Description of High-Energy and Low-Energy Data by TMDs with EXP and PDF Uncertainties

[Bury, Leal Gomez, Scimemi, Vladimirov, Zurita & H, arXiv:2201.07114]

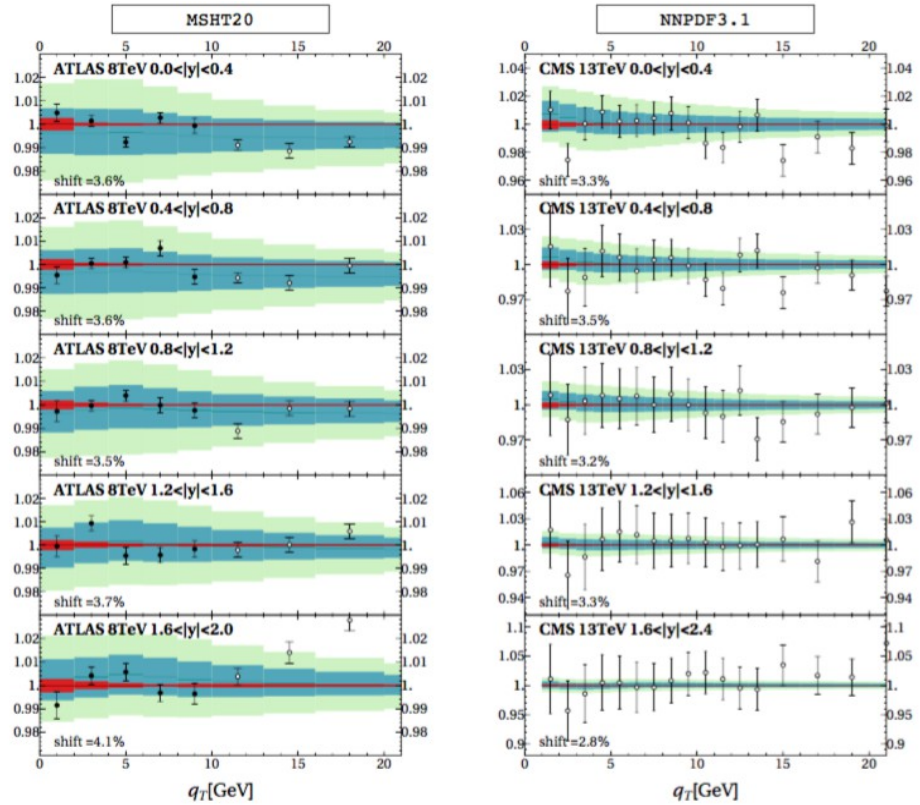

Figure 3: Example of the data description at high energy. Left panel: the ratio $d\sigma_{\text{experiment}}/d\sigma_{\text{theory}}$ for Z-boson production at 8 TeV measured by the ATLAS experiment with MSHT20. Right panel: the ratio $d\sigma_{\text{experiment}}/d\sigma_{\text{theory}}$ for Z-boson production at 13 TeV at the CMS experiment with NNPDF3.1. The red band is the **EXP**-uncertainty. The light-green band is the **PDF**-uncertainty. The blue band is the combined uncertainty. Only the filled bullets are included into the fit.

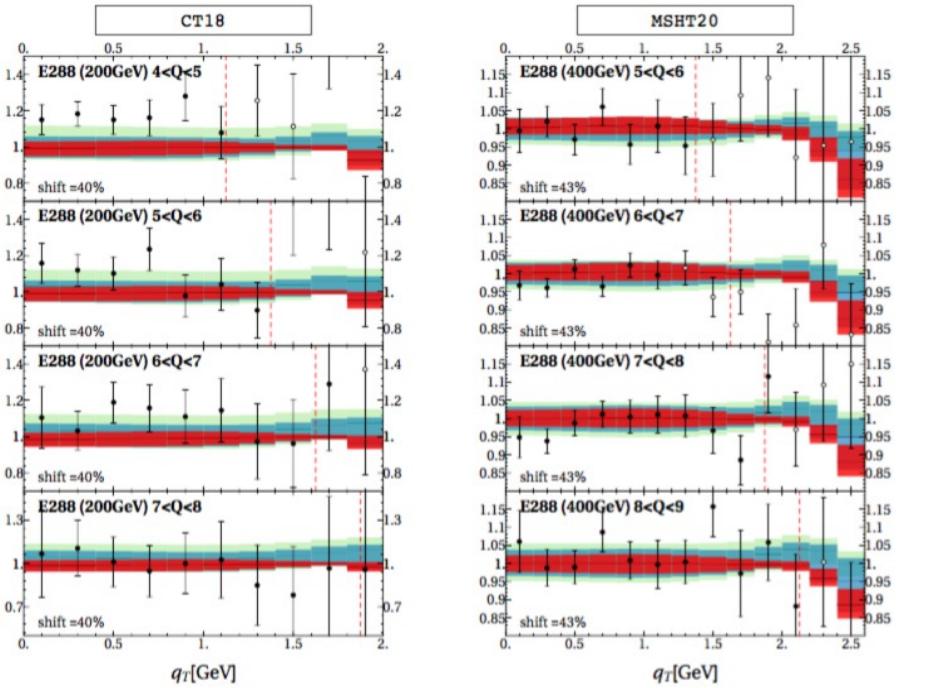

Figure 4: Example of the data description at low energy. Left panel: ratio $d\sigma_{\text{experiment}}/d\sigma_{\text{theory}}$ for the DY process at E288 experiment with 200 GeV beam-energy with CT18. Right panel: ratio $d\sigma_{\text{experiment}}/d\sigma_{\text{theory}}$ for the DY process at E288 experiment with 400 GeV beam-energy with MSHT20. Red band is the **EXP**-uncertainty. Light-green band is the **PDF**-uncertainty. The blue band is the combined uncertainty. The filled bullets are included into the fit. The dashed red vertical lines illustrate the cut $q_T < 0.25Q$ discussed at the beginning of sec. 3.

Perturbative Scale Variation

To better appreciate the role of the PDF and EXP uncertainty bands in figs. 3-4, we next consider the theoretical uncertainty bands obtained by variation of the perturbative scales. We perform the scale variation according to the ζ prescription approach in [6, 37]. This amounts to varying two scales, the factorization scale in the DY cross section formula and the small-b matching scale in the OPE expansion of the solution of TMD evolution equations. (The small-b matching scale of the CS-kernel is present in this approach but its variation is not included in the calculation.) We vary these scales by factors c in the range $[0.5, 2]$, and take the maximum symmetrized deviation. The resulting bands are shown in fig. 5.

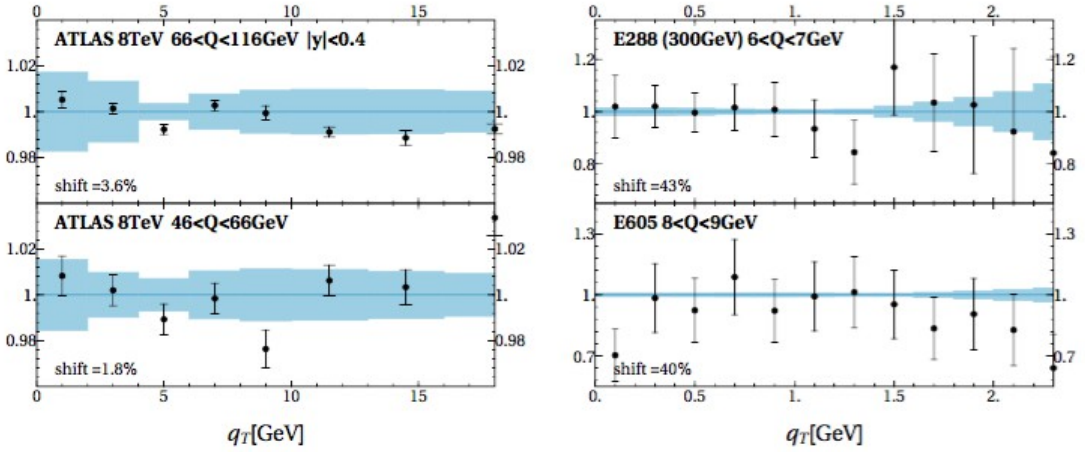

Figure 5: Scale variation band in comparison to typical data at high (left panel) and low (right panel) energies. The scale variation band is defined as the maximum symmetrized deviation from varying all scale parameters by a factor $c \in [0.5, 2]$.

We observe that the PDF uncertainty bands in fig. 3 are comparable or larger than the perturbative scale variation bands in fig. 5. This underlines that DY transverse momentum measurements in the TMD region are potentially useful to place constraints on PDFs. For this purpose one needs to employ a theoretical framework capable of describing the low transverse momentum region. One could envisage doing this in a resummation framework, formulated in terms of collinear PDF only, or in a TMD framework, in which a joined fit of both PDFs and TMDPDFs will put extra constraints on the PDFs.

Bury et al., arXiv:2201.07114

PDF replicas and qT shapes

- Does varying PDF replicas mostly result into a change in normalization of predictions for qT spectra?
  Not really: different PDF replicas induce different qT shapes.

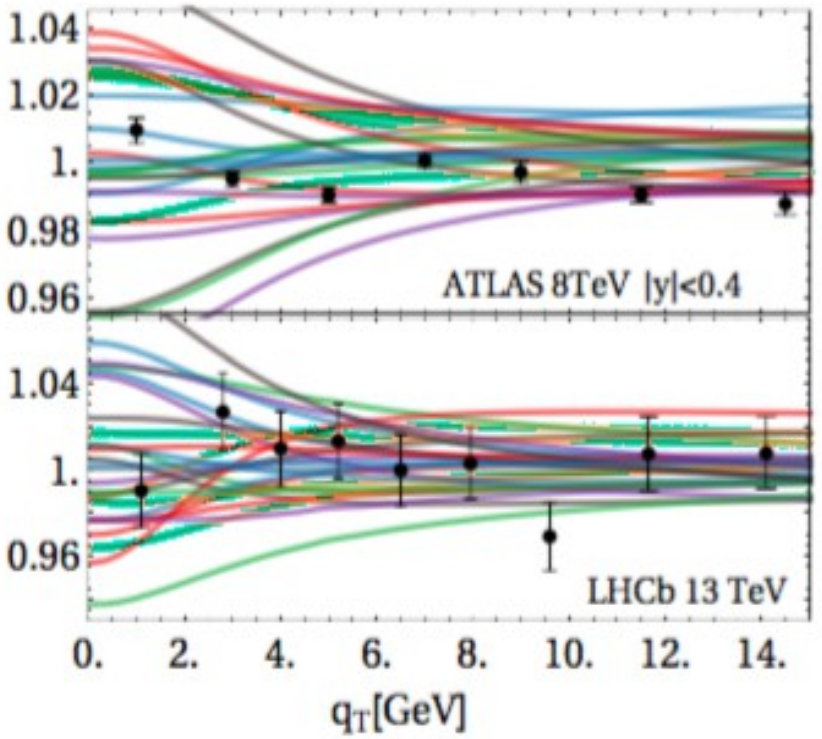

Figure 14: Examples of prediction using different PDF replicas at the same f_{NP}.

- This is at the origin of the chi-squared values spread among replicas observed earlier. It is due to the fact that the OPE relation couples the *b* and *x* dependences.

Extracted TMD distributions with inclusion of PDF uncertainty and flavor dependence

Bury et al., arXiv:2201.07114

- Differences between flavours are clear:
  - **Red** : EXP
  - **Blue** : PDF
  - **Black**: combined

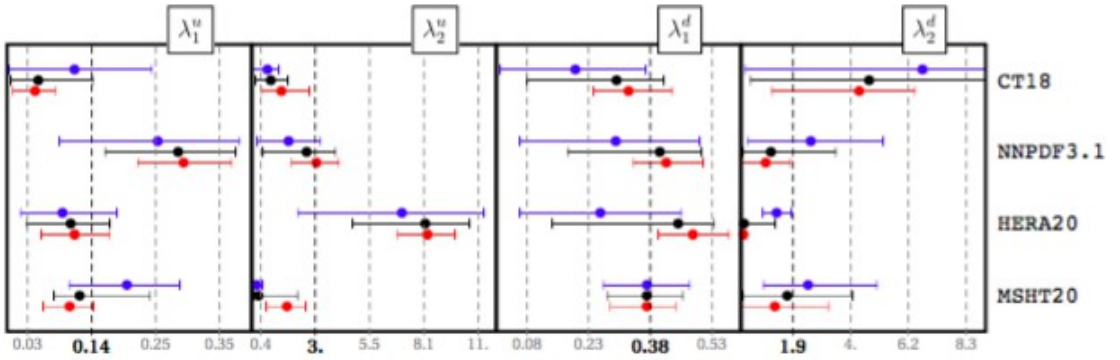

- We obtain realistic uncertainty bands for the TMDPDFs:

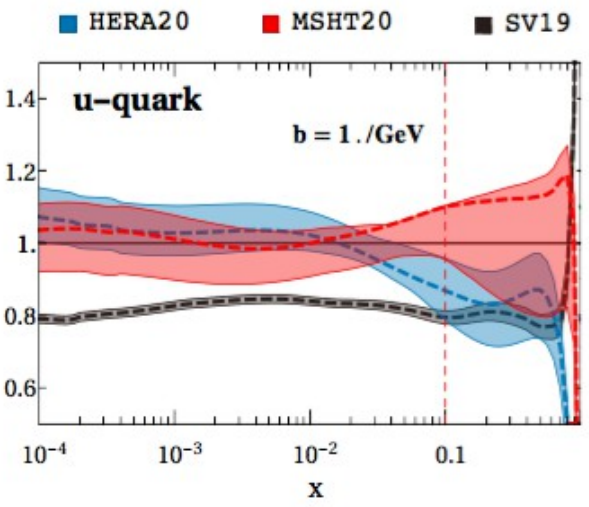

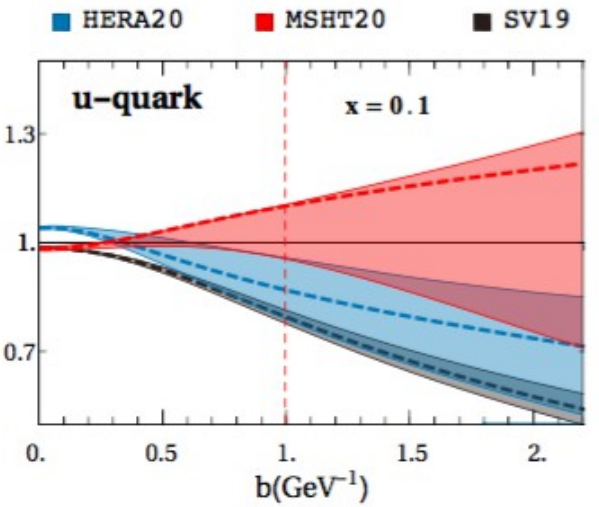

slide by P. Zurita

CONCLUSIONS

- Bayesian analysis to propagate PDF uncertainties to unpolarized TMDs: PDF uncertainties found to be larger than EXP uncertainties for all *b*.
- As a result of the improved analysis framework, the TMD error bands are significantly increased compared to previous fits based on OPE.
- This also impacts polarized TMD analyses, for which unpolarized cross sections are used to normalize angular distributions and asymmetries.
- Flavor dependence of NP TMD distributions included for the first time in fits based on TMD evolution: i) it reduces the spread in chi-squared distributions over replicas; ii) leads to more consistent results among different PDF sets.

EXTRA SLIDES

Correlation of TMD parameters for different PDF sets

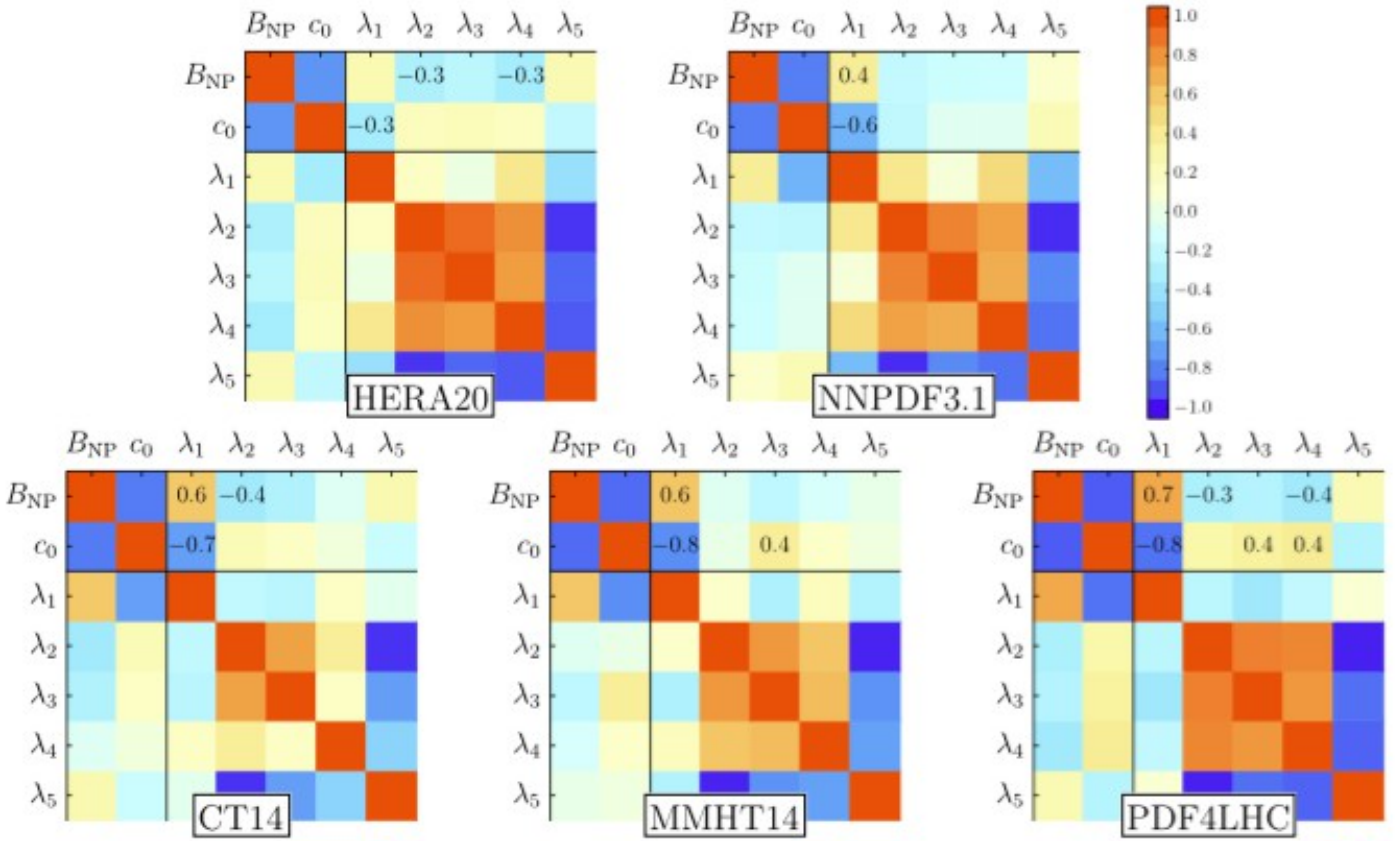

Fig. 3. Correlations of TMD fit parameters. In the axes $1 = B_{NP}$, $2 = c_0$, $(3, 4, 5, 6, 7) = \lambda_{1,2,3,4,5}$. Low correlation is represented by light colors, high correlation by dark colors. (The diagonal entries are trivial.)

- Correlations vary with PDF sets

The cut qT / Q < delta

- We vary the cut delta on the data set

- The delta dependence is mild between 0.1.and 0.25 both for the chi^2 and for the parameter values

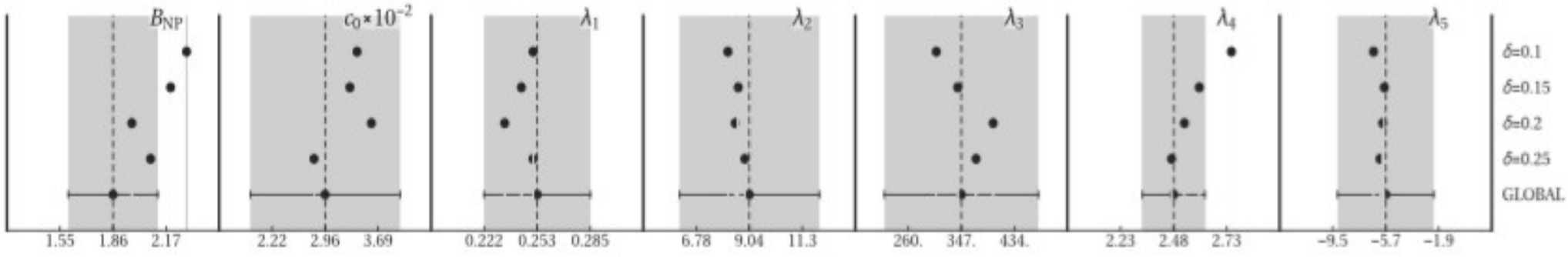

Fig. 2. Dependence of the values of the fitted TMD parameters on the δ cut (NNPDF3.1 PDF set).

- Matching with high qT region is not included yet

The role of precision LHC measurements

2-parameter fits (cases 1, 3, 5): no intrinsic kT
3-parameter fits (cases 2, 4, 6): both nonperturbative Sudakov and intrinsic kT

Case	B_{NP}	g_K	λ_1 ($f_{NP} = \exp -\lambda_1 b^2$)	χ^2/dof	χ^2/dof(norm.)
1	5.5 (max)	0.116 ± 0.002	10^{-3}(fixed)	3.29	3.04
2	2.2 ± 0.4	0.032 ± 0.006	0.29 ± 0.02	1.50	1.28
Case	B_{NP}	c_0	λ_1	χ^2/dof	χ^2/dof(norm.)
3	1. (min)	0.016 ± 0.001	10^{-3}(fixed)	2.21	1.99
4	3.0 ± 1.5	0.04 ± 0.02	0.27 ± 0.04	1.61	1.36
Case	B_{NP}	g_K^*	λ_1	χ^2/dof	χ^2/dof(norm.)
5	1.34 ± 0.01	0.16 ± 0.01	10^{-3}(fixed)	1.70	1.52
6	2.43 ± 0.66	0.05 ± 0.02	0.24 ± 0.04	1.49	1.28

Table 3: Results of 3-parameter and 2-parameter fits. The PDF set used is NNPDF3.1 [63].

- 3-parameter cases similar to global fit results
- Case 6: saturating behavior d D / d ln b = 0

$$R_\sigma = 2\,\frac{d\sigma^{\text{test}} - d\sigma^{TMD}}{d\sigma^{\text{test}} + d\sigma^{TMD}}\,, \qquad (12)$$

- 2-parameter fits lead to higher chi2 values and different fitted parameters for rapidity kernel.
- I.e., intrinsic kT effects may be reabsorbed by changes in D.

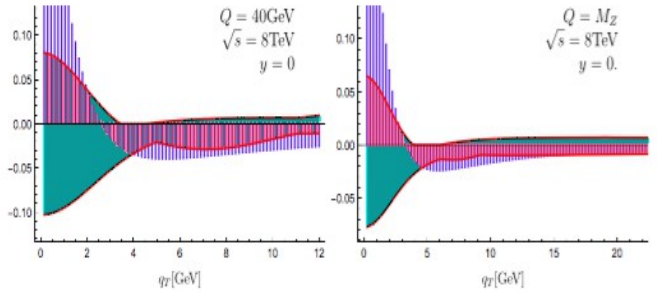

Figure 4: Sensitivity to nonperturbative physics in LHC DY measurements: the transverse momentum dependence of the ratio in Eq. (12), for central rapidity and different values of the lepton-pair invariant mass. The solid band is obtained from perturbative scale variation.

Given the reduction of perturbative uncertainties due to high logarithmic accuracy, residual uncertainty from nonperturbative TMD effects is non-negligible at low qT and increasing with decreasing masses.

Nonperturbative contributions I: rapidity evolution kernel

- Write D using b* prescription as

$$\mathcal{D}^f(\mu, \boldsymbol{b}) = \mathcal{D}^f_{\text{res}}(\mu, b^*(\boldsymbol{b})) + g(\boldsymbol{b}), \qquad \text{where} \qquad b^*(\boldsymbol{b}) = |\boldsymbol{b}| \sqrt{\frac{B_{\text{NP}}^2}{\boldsymbol{b}^2 + B_{\text{NP}}^2}}$$

- Nonperturbative component of rapidity evolution kernel modeled and fitted to data:

$$g(\boldsymbol{b}) = g_K \boldsymbol{b}^2,$$

quadratic behavior
(traditionally used in TMD fits since Resbos)

$$g(\boldsymbol{b}) = c_0 |\boldsymbol{b}| b^*(\boldsymbol{b}),$$

linear rise at large b

$$g(\boldsymbol{b}) = g_K^* \boldsymbol{b}^{*2},$$

quadratic at small b, constant at large b
(similar spirit to parton saturation in s-channel picture *[Soper & H, PRD 75 (2007) 074020]*)
d D / d ln b = 0 for large b

- Zeta prescription scale setting *[A. Vladimirov, arXiv:1907.10356]*

$$\zeta_{\text{NP}}(\mu, b) = \zeta_{\text{pert}}(\mu, b) e^{-b^2/B_{\text{NP}}^2} + \zeta_{\text{exact}}(\mu, b)\left(1 - e^{-b^2/B_{\text{NP}}^2}\right).$$

RAPIDITY EVOLUTION KERNEL

- Red curves: quadratic D; yellow curves: saturating D; blue curves: linear D.
- For each color, difference between solid and dashed curves measures correlations between Sudakov and intrinsic kT effects.

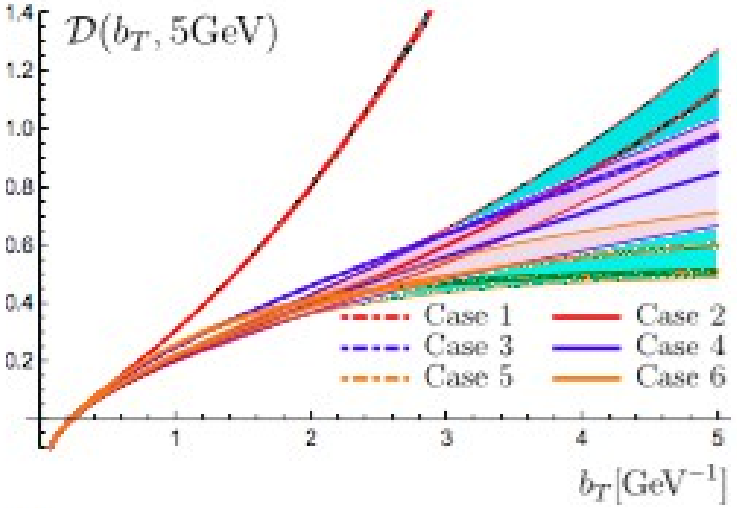

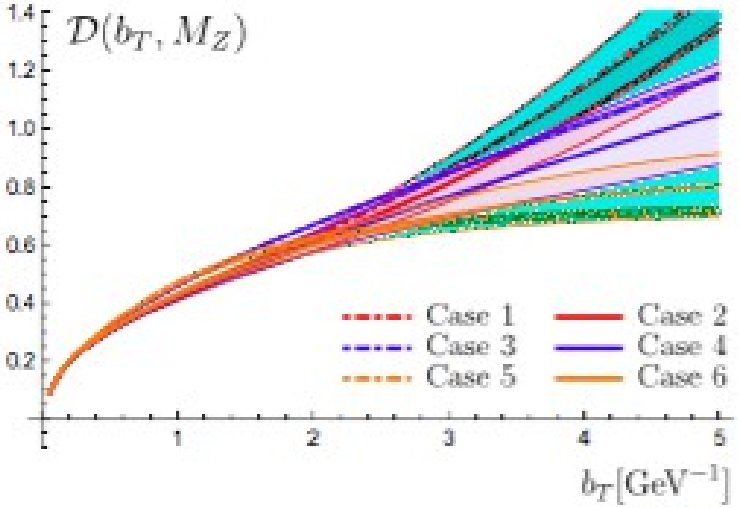

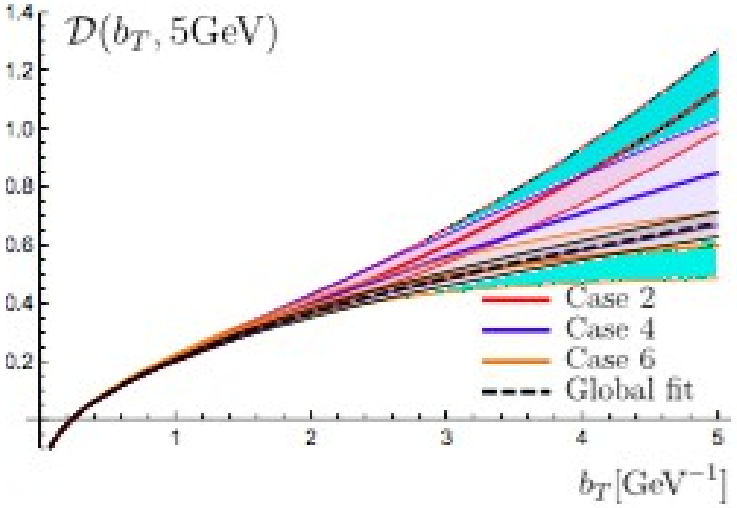

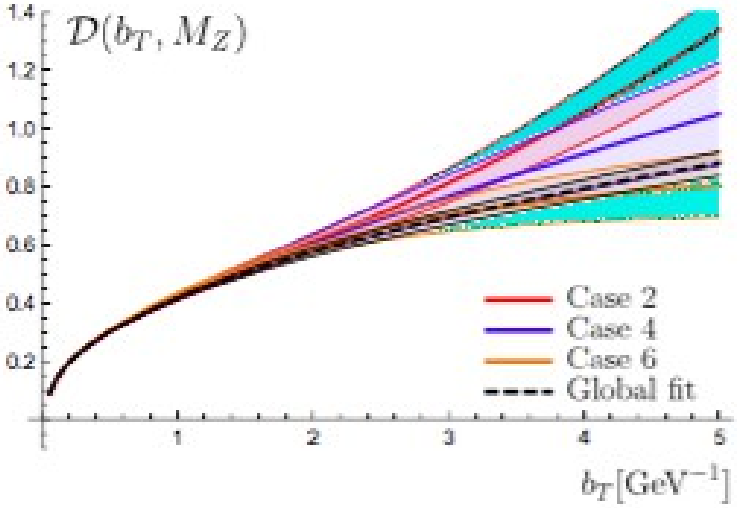

Quadratic model implies more pronounced dependence on intrinsic kT than the others (showing up especially for low masses)

RAPIDITY EVOLUTION KERNEL

- Limited sensitivity of current LHC measurements to long-distance region results into sizeable uncertainty bands at large b
- Higher sensitivity from low-qT measurements with fine binning in qT at low masses

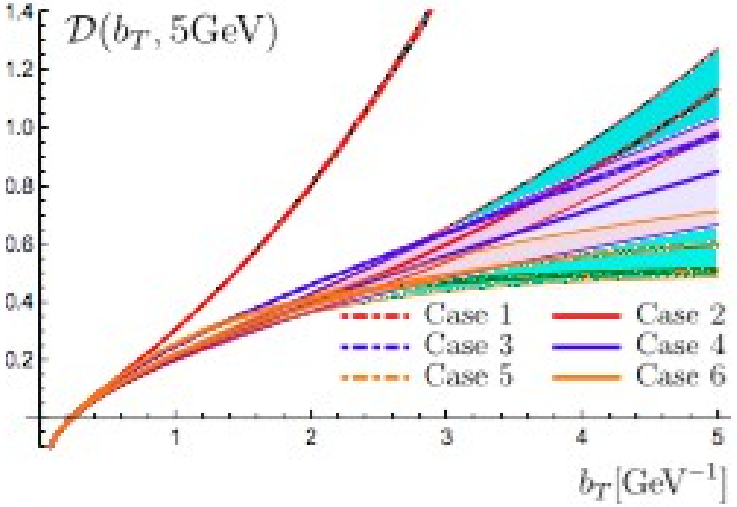

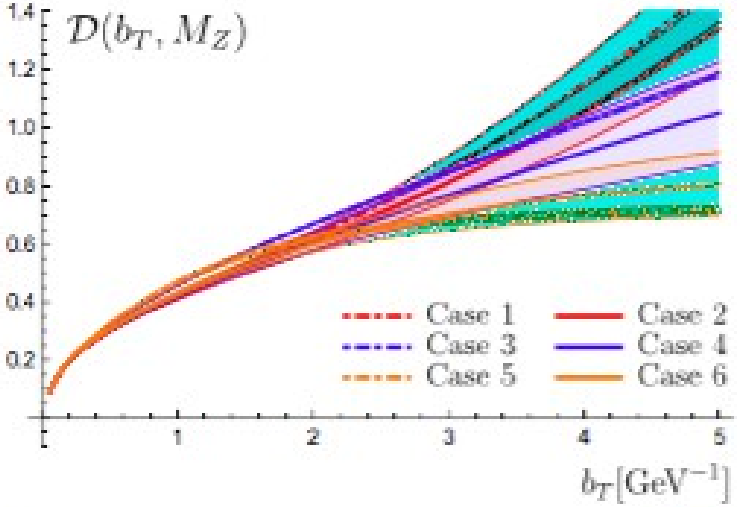

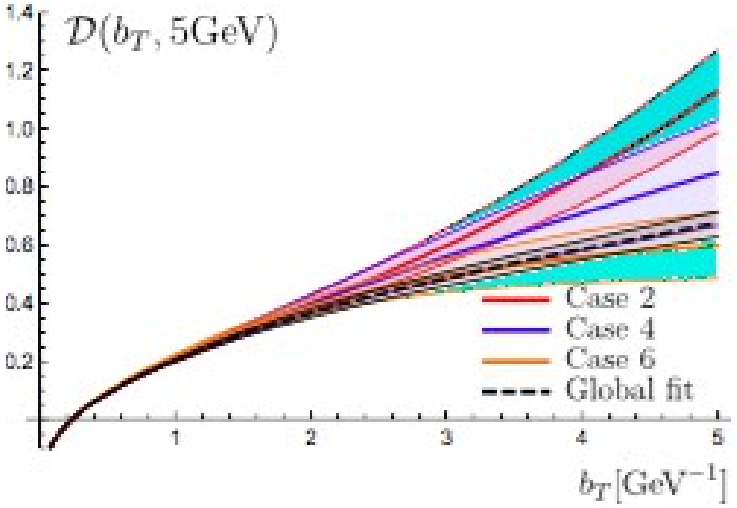

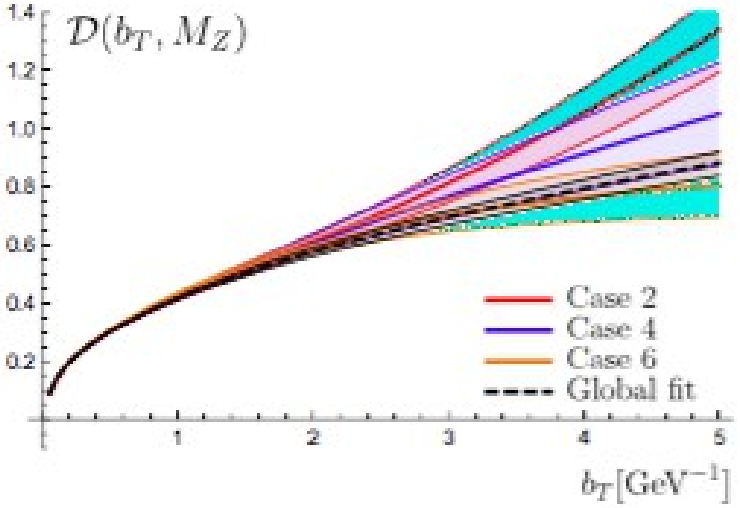

- Global fit result in lower panels illustrates role of low-energy data: performed with linear model – but lower than blue curve and closer to yellow (saturating) curve

Remarks

- Used low-qT TMD factorization to investigate sensitivity of LHC and low-energy DY measurements to nonperturbative f and D, and correlations with collinear PDFs.
- Although strongest nonperturbative sensitivity is from low energy, neglecting any intrinsic kT at the LHC worsens quality of fits and causes potential bias in determination of rapidity evolution kernel
- Residual uncertainty from nonperturbative TMD effects non-negligible in lowest qT bins (increasing with decreasing masses)
- Results on large-b behavior of rapidity evolution kernel complementary to lattice studies – e.g. linear vs. saturating behavior
- Matching with high qT region yet to be included

Inclusion of PDF uncertainty in TMD extraction

- EXP: 100 replicas of the data.
- PDF: 1000 replicas of the PDFs.

- For each case we obtain a set of parameters which are then combined in a weighted average to give the final result.

- More importantly:

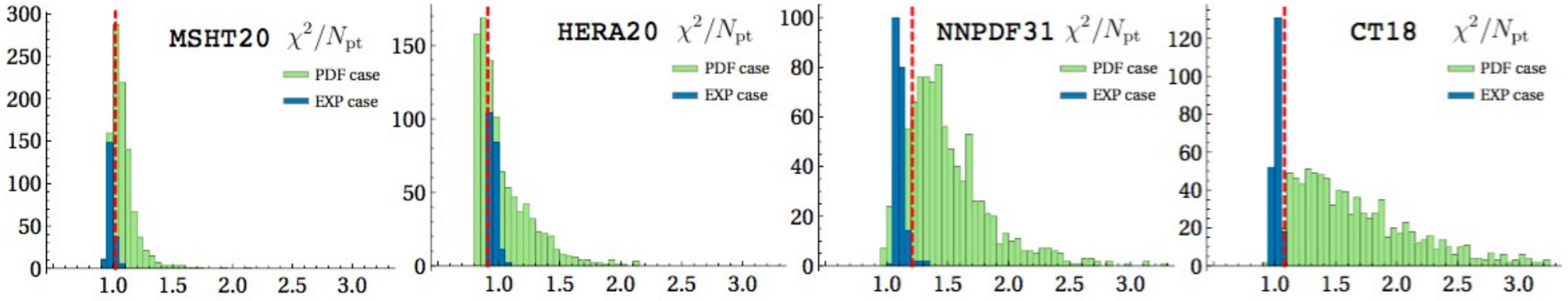

Extracted TMD parameters

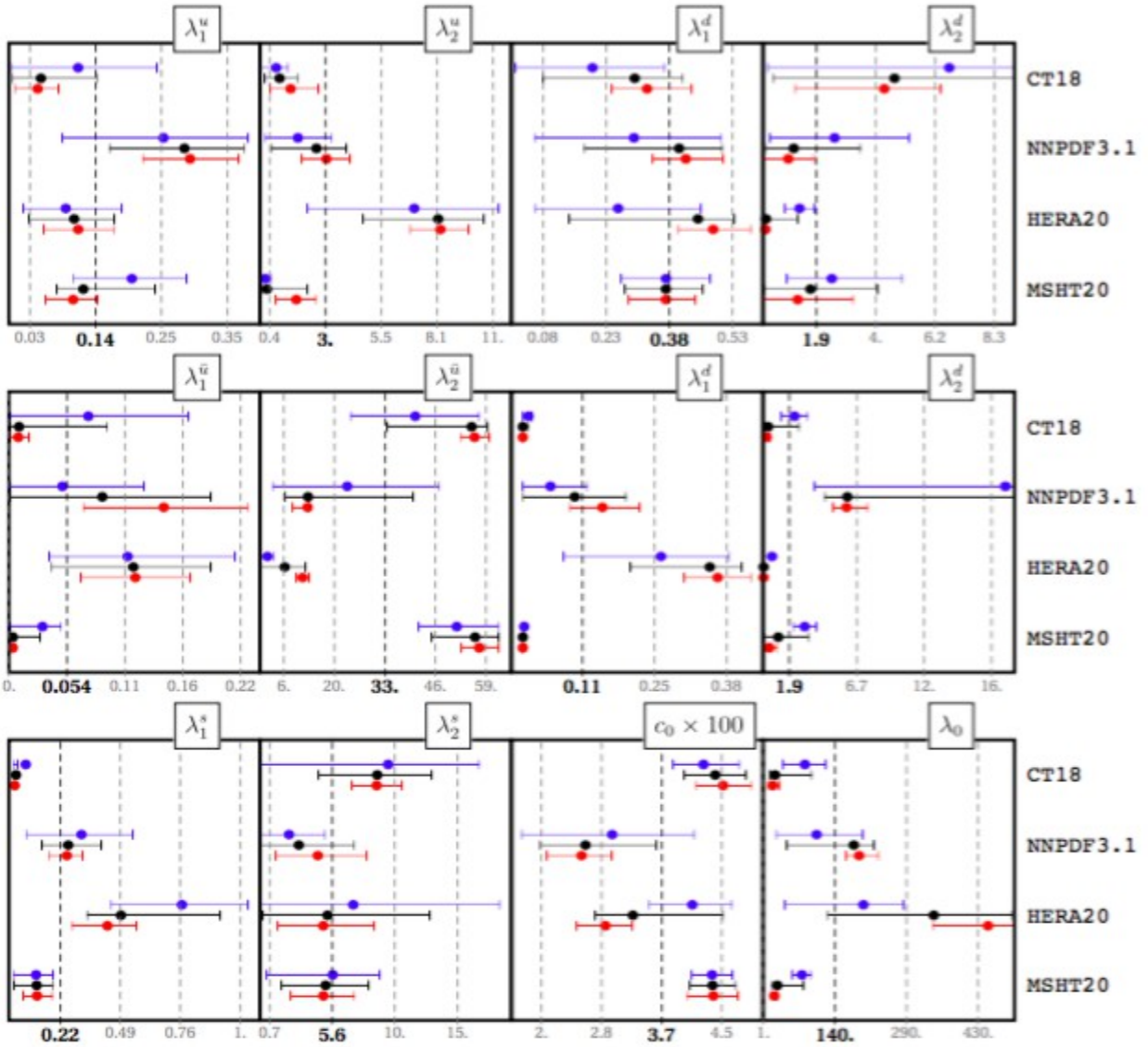

Figure 8: Comparison of the parameter values. Black is the final result. Blue is the value from the fit of the **PDF** case. Red is the value from the fit of the **EXP** case.

TMD uncertainties

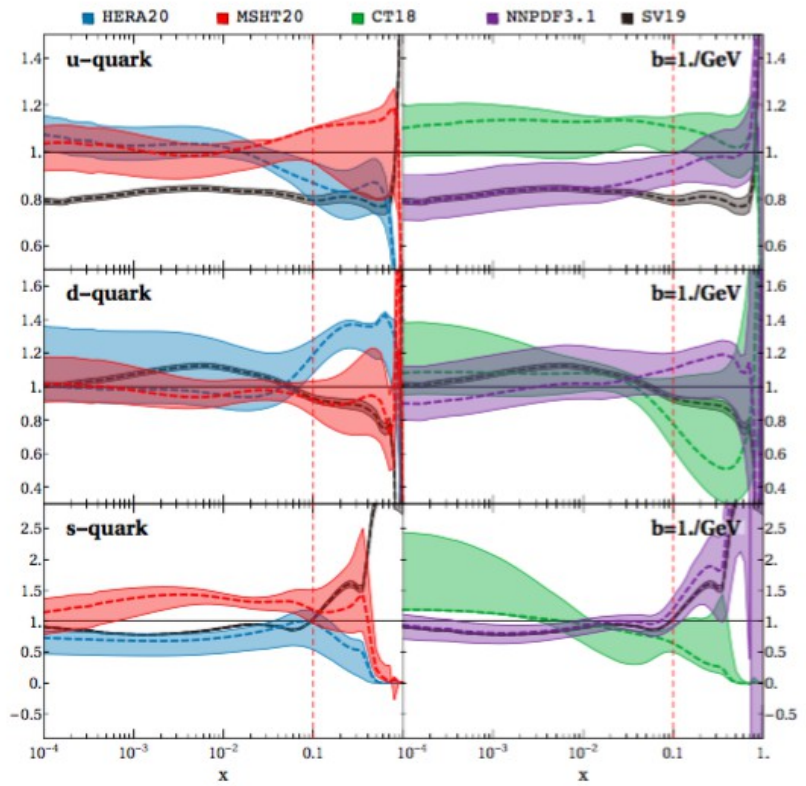

Figure 10: Comparison of uncertainty band for unpolarized TMDPDFs extracted with different PDFs. Here, the slice of optimal TMDPDF at $b = 1\text{GeV}^{-1}$ is shown as the function of x. For convenience of presentation the plot is weighted with the central TMDPDF value averaged between different PDF cases. The red line indicates the position of slice demonstrated in fig.11.

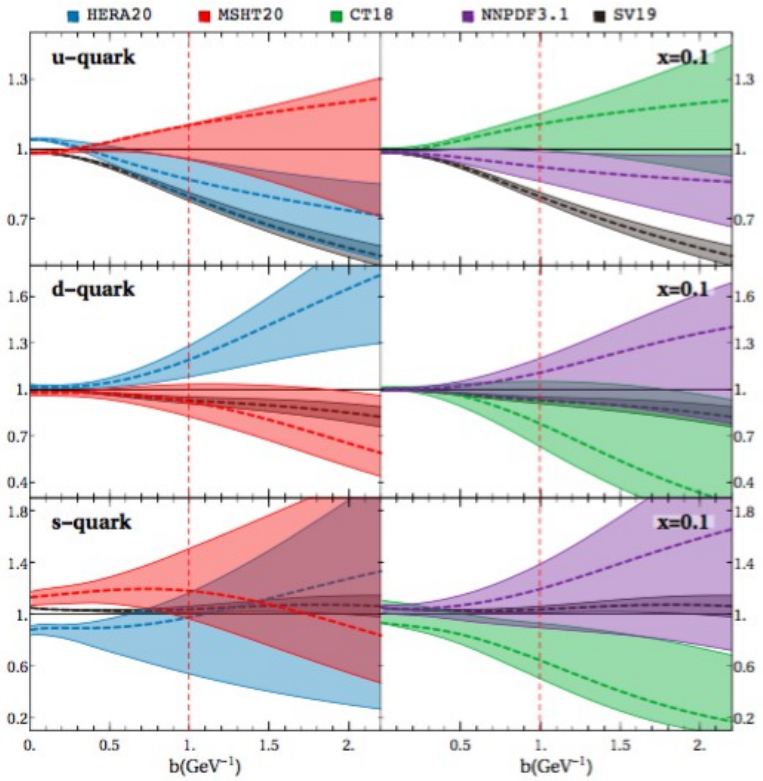

Figure 11: Comparison of the uncertainty band for unpolarized TMDPDFs extracted with different PDFs. Here, the slice of optimal TMDPDF at $x = 0.1$ is shown as a function of b. For convenience of presentation the plot is weighted with the central TMDPDF value averaged between different PDF cases. The red line indicates the position of slice demonstrated in fig. 10.